Simulation of tensile tests of hemp fibre using discrete element method

M. A. Sadek[1], L. Guzman[1], Y. Chen[1*], C. Laguë[2], H. Landry[3]

(1. *Department of Biosystems Engineering, University of Manitoba, Winnipeg, Manitoba R3T 5V6, Canada;*
2. *Faculty of Engineering, University of Ottawa, Ottawa, Ontario, K1N 6N5, Canada;*
3. *Prairie Agricultural Machinery Institute, Humboldt, Saskatchewan, S0K 2A0, Canada*)

Abstract: Tensile strength is an important property of hemp fibre, because it determines the mechanical strength of fibre-based products such as biocomposites. Commercial discrete element software, Particle Flow Code in Three Dimensions (PFC^{3D}), was used to develop a numerical model which simulates tensile tests of hemp fibre. The model can predict the tensile properties (such as strength and elongation) of a hemp fibre. In the model, a virtual hemp fibre was defined as a string of spherical balls, held together by cylindrical bonds implemented in PFC^{3D}. To calibrate the model, tensile data was collected for both unretted and retted hemp fibres using a commercial Instron testing system. The average fibre diameter was 0.34 mm for the unretted fibre and 0.30 mm for the retted fibre. The average tensile strength measured was 358 MPa for the unretted fibre and 343 MPa for the retted fibre. The corresponding average elongations for the two types of fibres were 0.88 and 0.80 mm, for an original fibre length of 25 mm. The bond modulus, the most sensitive microproperty of the model was calibrated. The calibrated value was 1.02×10^{10} Pa for unretted fibre and 1.05×10^{10} Pa for retted fibre. Using the calibrated bond modulus, elongations of fibre were simulated using the model. The simulation results showed that the elongation increased linearly with the increasing fibre length; whereas the elongation was not affected by the fibre diameter.

Keywords: hemp, fibre, PFC^{3D}, tensile, strength, elongation, simulation

Citation: Sadek M. A., L. Guzman, Y. Chen, C. Laguë, H. Landry. 2014. Simulation of tensile tests of hemp fibre using discrete element method. Agric Eng Int: CIGR Journal, 16(2): 126−135.

1 Introduction

Hemp fibre is a valuable source for making environmentally friendly and biodegradable products. Also, hemp fibre has very high tensile strength ranging between 0.49 to 1 GPa (Williams and Wool, 2000; Munder and Fürll, 2004; Beckermann and Pickering, 2008). As a result, hemp fibre has been used in many applications such as textile products and bio composites for automobile industries. Development of any hemp fibre products requires the knowledge of physical and mechanical properties of hemp fibre. Hemp fibre is the outer layer of the hemp stem, also called bast fibre (Garcia et al., 1998; Mediavilla et al., 2001). Bast fibres consist of individual fibres which are bonded together by an interface, which contains mainly cellulose (67%), hemicelluloses (13%); and lignin (4%) (Bocsa and Karus, 1997; Keller et al., 2001). These groups of joined single fibres are known collectively as fibre bundles, and are responsible for making up the bark tissue. This study did not deal with single fibres, but with fibre bundle (referred to as fibre hereafter for simplicity).

Tensile strength is one of the important fibre properties because of its extensive use in evaluating the strength of fibre products (Bledzki et al., 1996). Tensile strength of hemp fibre may be affected by chemical treatment (Beckermann and Pickering, 2008) and retting of the hemp (Munder and Fürll, 2004). Retting is a biological process by which pectin and hemi cellulosic

Received date: 2013-02-21 **Accepted date:** 2014-02-17
Corresponding author: Ying Chen, Department of Biosystems Engineering, University of Manitoba, Winnipeg, Manitoba R3T 5V6, Canada. Email: ying_chen@umanitoba.ca. Tel.: 1 204 474 6292; fax: 1 204 474 7512.

compounds between the individual fibre cells are degraded. Although fibre properties have been measured by several researchers (Rowell et al., 2000; Hobson et al., 2001; Munder and Fürll, 2004), little work has been done to numerically simulate fibre tensile properties (Sadek et al., 2011).

This study used the discrete element method (DEM) to simulate tensile tests of hemp fibre to predict the tensile properties of the fibre. The DEM is a numerical method to model a material as an assemblage of discrete particles. The DEM was first introduced by Cundall and Strack (1979) for analyzing geological materials (rocks and soils). Since then, the DEM has become a promising tool to simulate mechanical behaviours of various other materials, including hemp fibre (Sadek et al., 2011). However, no simulations have been carried out on tensile tests of hemp fibre using the DEM.

Commonly used DEM software is Particle Flow Code in Three Dimensions (PFC^{3D}) (Itasca Consulting Group, Inc., Minneapolis, MN). In PFC^{3D}, the basic particles are spherical and they are referred to as balls. Materials to be simulated are represented by assemblies of individual balls. PFC^{3D} provides users with different contact models among particles, which allows to model different particle interaction behaviours, for example, free-flowing granular material, such as powder and grains (Djordjevic, 2003; Sakaguchi et al., 2001), cohesive and frictional materials, such as soil and manure (Mak et al., 2012; Landry et al., 2006), and solid materials, such as rock (Potyondy and Cundall, 2004; Pierce, 2004). PFC^{3D} is considered to be one of the effective tools for the simulation of hemp fibres.

Regardless of the type of material to be simulated, a set of microproperties is required as input parameters for any DEM models. Microproperties define a model at the particle level, and they significantly affect the model outputs. Most microproperties are not measurable at the current time, and they are determined either using analytical assumptions or inverse calibration methods. In analytical assumption methods, microproperties are determined using existing theory of the material. For example, Young's modulus and Poisson's ratio of bulk material were used to determine particle normal and shear stiffness of the material (Cundall and Strack, 1982; Chang et al., 2003). In inverse calibration methods, microparemeters are determined by matching the simulated results with experimental data. For example, direct shear tests were used to calibrate model microproperties of a material through matching simulated friction angles with measured ones (Coetzee and Els, 2009; Sadek et al., 2011). Similarly Tanaka et al. (2000) and Asaf et al. (2007) used penetration test data for calibrating a soil model, and Vu-Quoc et al. (2000) used drop weight test data for calibrating a model for soybean grains.

In summary, understanding the tensile properties of hemp fibre is important to industries which use hemp fibre for their products. To date, no discrete element models have been developed for simulations of the fibre tensile properties. The objectives of this study were to (1) measure tensile properties of hemp fibres, (2) develop a discrete element model to simulate the tensile tests of hemp fibre using PFC^{3D}, and (3) calibrate the model using measurements, and simulate the tensile properties of hemp fibres of different diameters and lengths.

2 Mesurements of fibre tensile properties

2.1 Materials and methods

2.1.1 Tensile testing system

The Instron electromechanical testing system (3366, Instron Corporation, MA, USA) was used for fibre tensile tests. The testing system (Figure 1) consisted of a frame, a crosshead, two clamps, a load cell, a drive system, and a controller. The bottom clamp was stationary and affixed to the base of the frame, and the top clamp was connected to the crosshead through the load cell (2 kN capacity). The test fibre sample was secured using the clamps. As the drive system moved the crosshead up, it applied a tensile load on the sample. The system was controlled via Instron proprietary software (Bluehill2) which allowed users to set the test parameters and analyse the data.

2.1.2 Fibre sample preparation

Hemp fibre samples used for tensile tests were from two types of fibre: unretted and retted hemps. The unretted hemp was baled shortly after being swathed and the retted hemp was left to ret in the field for

approximately six weeks prior to being baled. In total 30 retted and 30 unretted samples were picked up from processed hemp (Figures 2a and 2b). Selected fibres were cut to a length of approximately 45 mm, and they were assigned an identification number from 1 to 30 (Figure 2c) for the purpose of randomizing the tests. The humidity of the environment where the measurements are taken has a significant effect on the strength and strain of textile materials (Saville, 1999). Therefore, before tensile tests, all fibre samples were exposed to a relative humidity of 65% and a temperature of 21ºC (CGSB, 2001) in an environmental chamber for three days.

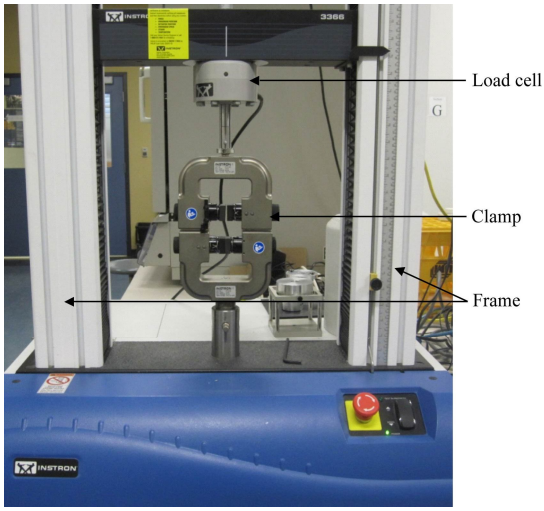

Figure 1 The Instron testing system and its components

a. Processed unretted hemp b. Processed retted hemp

c. Hemp fibre samples prepared for the tensile tests

Figure 2 Hemp materials

2.1.3 Tensile tests

Prior to the test, each fibre sample was attached to a thin cardboard frame (Figure 3a) to avoid slippage from the clamps of the testing system during pulling. Samples were straightened without pulling too hard and were secured inside the cardboard window using polyepoxide (Epoxy) glue. The window gave an effective testing fibre length of 25 mm. To start testing, the cardboard frame was fitted into the grips. Then the sides of the cardboard frame were cut so that only the fibre was pulled during the test. The clamps were attached at the inner edge of the card board, thus the glued fibre did not contribute to the measuring of fibre properties. Tension was applied to the fibre by moving the crosshead up at 2 mm/min and continued until the sample broke as shown in Figure 3b.

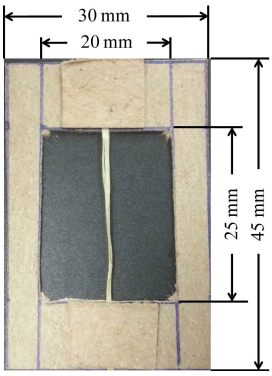

a. A fibre sample on a cardboard frame before test

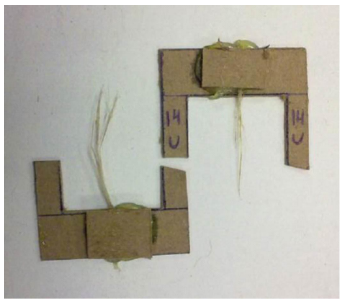

b. A broken fibre sample after test

Figure 3 Tensile testing samples

2.1.4 Measurements

The unit of fibre fineness is expressed as tex which is equal to a mass of 1 gram per kilometre of fibre length (Kymäläinen, 2004). The mass of the fibres was measured using a high-precision analytical scale (Symmetry PA 220, QC, Canada), and the length was measured using a ruler. The mass and the length were used to determine the fineness. Then, fibre diameter was estimated using the following equation, assuming that fibre had a circular cross-section (Munder and Fürll, 2004) and a uniform section along the length.

$$d = \sqrt{\frac{4f}{\pi\rho}} \quad (1)$$

where, d = fibre diameter, μm; f = fibre fineness, tex; ρ = fibre particle density, kg/m^3.

Particle density of hemp fibre was taken as 1,480 kg/m^3. This density value was reported by Lilholt and Lawther (2000).

The Bluehill2 software of the Instron testing system recorded the load-extension curve during a test. The sensitivity of the software was adjusted to determine the maximum load at 10% after drop in maximum force. Consequently, the software detected the maximum load at the fibre failure. Several parameters were derived to characterize the fibre properties with the recorded load-extension curve. The fibre strength was described in stress format. The maximum stress was the ratio of maximum tensile force and the cross-section area. The specific stress was the ratio of maximum tensile force and the fineness of the fibre (Khan et al., 2011). This parameter provides the means of comparing individual fibres in equivalent terms and methodology. The maximum strain was the relative change in length of the sample at the maximum tensile force, recorded by the Bluehill2 software. The elongation at the fibre failure was determined from the maximum strain, given the initial fibre length of 25 mm. The software used a least square fit algorithm to determine the modulus of elasticity from the load-extension curve. The criteria for measuring the modulus of elasticity was implemented by an algorithm built within the Bluehill2 software. The modulus of elasticity in this study was expressed in the same units as the specific stress. To determine the work of rupture, the Bluehill2 software measured the amount of energy required to reach the yield point; this energy was calculated by determination of the area under the load-extension curve before the yield point. The yield point is the point where the slope of the load-extension curve is zero.

2.2 Data processing

Out of 30 fibre samples tested, the data considered valid included 21 samples for the unretted fibres and nine samples only for the retted samples. In instances where the glue was not able to maintain the sample attached to the cardboard frame, the data were discarded. It is important to note that the main objective of the tensile tests in this study was to support model development. Therefore, in spite of the limited number of fibre samples, the data was deemed sufficient for the purpose of model calibration. Student's t-tests were used to examine differences in those measured variables between the retted and unretted fibres at the probability of 0.05.

2.3 Results and discussion

2.3.1 Load-extension curve

Load-extension (elongation) curves from the tensile tests could be classified into three types of curves. One type showed the brittle behaviour of hemp fibre. As the fibre was extended, the load increased in a linear fashion; at a certain point of extension, the load reached its peak, and the fibre sample suddenly broke and the load dropped to zero (Figure 4a). For the particular fibre shown in Figure 4a, the tensile strength and the elongation of the fibre were 30 N and 0.65 mm, respectively. Another type of curve also showed the brittle behaviour; however, the increasing load portion of the curve was not linear, but polynomial (Figure 4b). The third type of curve had the similar increasing portion (in either linear or polynomial fashion), but a gradual failure pattern (Figure 4c). In the last case, the fibre must be split into multiple thinner fibres which broke at different times during testing, and the incompletely broken fibre could still carry some load until being completely broken.

For the unretted fibres, the majority (approximately 80%) of the samples behaved like either Figure 4a or Figure 4b, and the other 20% behaved more like Figure 4c. For the retted fibres, approximately 50% experienced a form of behaviour like Figure 4a, and the other 50% behaved like Figure 4c. One can say that the unretted fibres were more brittle than the retted fibres. However, this will need to be verified further with a larger number of samples.

2.3.2 Fibre properties

The results of statistical analysis showed that none of the measured variables were significantly different between the retted and unretted fibres at the probability of 0.05. This was due to the highly variable nature of fibre properties, as indicated by the high standard deviations of the measurements shown in Table 1. However, the data showed some important trends in the effects of retting conditions on fibre properties.

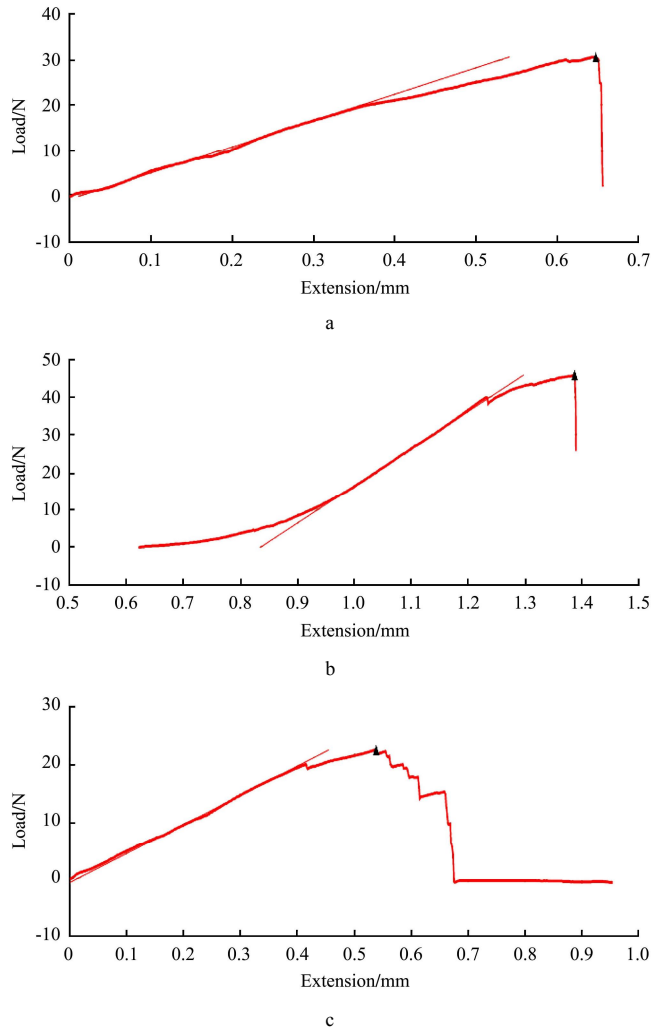

Figure 4 Typical results of load-extension curves from the tensile tests: (a) linear curve and sudden failure, (b) polynomial curve and sudden failure, (c) gradual failure; the triangle sign on the figure stands for the point where the maximum load and strain were taken

Table 1 Summary of measured properties of the unretted and retted fibres

Property	Unretted fibre		Retted fibre	
	Mean	SD[1]	Mean	SD[1]
Fineness, tex	139	59.6	107	39.0
Diameter, mm	0.34	0.071	0.30	0.057
Maximum load, N	31.6	15.6	24.5	15.9
Maximum stress, MPa	358	173	343	157
Specific stress, cN/tex	24.2	11.7	23.2	10.6
Maximum strain, %	3.55	1.78	3.20	2.34
Elongation, mm	0.88	0.44	0.80	0.58
Work of rupture, mJ	17.1	14.4	12.9	14.6
Modulus, cN/tex	1136	651	1397	603

Note: [1]SD is standard deviation.

The retted fibre had approximately 23% lower fineness and 35% lower standard deviation than the unretted fibre (Table 1). This indicated that retting hemp could improve the fineness and the uniformity of fineness. Accordingly, the diameters of the retted fibre were smaller and less variable than those of the unretted fibre. On an average, the retted fibre carried 22% lower loads than the unretted fibre, the corresponding maximum loads were 24.5 and 31.6 N respectively. Although the retted fibre had smaller diameter and lower fineness, only 4% lower maximum stress and 8% lower specific stress were observed for the retted fibre. Similar specific stresses were reported by Khan et al. (2011) for unretted fibres. Munder and Fürll (2004) found that the maximum tensile stresses of hemp fibre varied from 0.5 to 0.9 GPa, which were slightly higher than those observed in this study. Higher specific stresses were also reported by Hobson et al. (2001) for retted and unretted hemp fibre.

The maximum strain and elongation of the retted fibre were also slightly lower, when compared to those of the unretted fibre. As a result of their lower loads and strains, the retted fibre had lower work of rupture and higher modulus. Sankari (2000) studied the properties of 14 varieties of hemp fibres and reported higher specific stresses ranging from 41 to 74 cN/tex, but the reported maximum strains (3.3% to 5.0%) were similar to this study.

3 Simulations of fibre tensile properties

3.1 Model development

3.1.1 Construction of virtual fibre

For simulations of tensile tests, a virtual fibre was constructed with a set of PFC^{3D} basic particles (balls). In PFC^{3D}, particles can be connected together into clusters or clumps. Cluster is a group of balls which are connected by bonds, and they are breakable with external forces. Clumps are also group of balls, but they are not breakable under external forces. Therefore, clumps do not reflect modelled fibre materials. In this study, a virtual fibre was represented by a cluster of balls which were arranged like a string (Figure 5a). All the balls had the same diameter. The ball diameter and number of balls can be varied to match the diameter and length of the fibre to be simulated. The number of balls required for a fibre with a given length and a given diameter is calculated by the following equation:

$$n = \frac{l}{D} + 1 \tag{2}$$

where, n = number of balls in the virtual fibre; D = diameter of balls, equal to the diameter of fibre, mm; l = length of virtual fibre, mm.

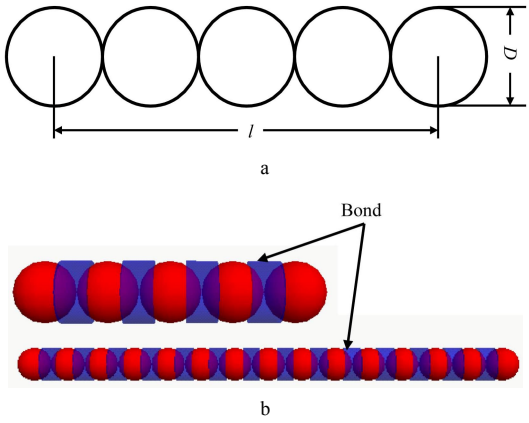

Figure 5 Virtual fibres: (a) dimensions of a virtual fibre, l is fibre length, and D is fibre diameter; (b) examples of PFC^{3D} virtual fibres

The next step was to define the contact between balls in the virtual fibre, so that the virtual fibre could withstand tensile load like a real fibre. The PFC^{3D} parallel bond models (PBM) are suitable for this purpose, because the bond at the contact between balls provides certain inter-particle tensile capacity. Examples of virtual fibres with the PBM are shown in Figure 5b. Bond acts over a circular cross section at the contact point of two balls, and the radius of the cylindrical bond is equal to the radius of the ball. The cylindrical bond withstands tensile load, and the bond breaks if the maximum external load exceeds the prescribed strength of the bond (Potyondy and Cundall, 2004). Breaking of any bonds in a virtual fibre means the failure of the virtual fibre. Therefore, the strength of the virtual fibre is determined by the properties of the bond to be specified by users.

3.1.2 Microproperties of virtual fibre

When using the PFC^{3D} PBM, material to be modelled is defined by three ball microproperties: normal stiffness (k_n), shear stiffness (k_s), and friction coefficient (μ), and five bond microproperties: the radius of the cylindrical bond (R), normal and shear stiffness ($\bar{k}^n$ and $\bar{k}^s$), normal and shear strength (σ_c and τ_c). In the case of a fibre subjected to a tensile load, the bond microproperties are more relevant than the ball microproperties as the balls are connected with bonds only, and there is no interaction among the balls under tensions. The value of R was set to be equal to the ball radius, as illustrated in Figure 5b. To reduce the number of bond microproperties to be calibrated, τ_c was set to be equal to σ_c, and $\bar{k}^n$ was set to be equal to $\bar{k}^s$. The same assumptions have been made in the literature for modelling other materials (Asaf et al., 2007; McDowell and Harireche, 2002). On the other hand, τ_c and $\bar{k}^s$ are not critical in this particular case having tensile load only. The stiffness of the isotropic linear elastic material is related to the modulus and varies with the particle size. Then, the stiffness was calculated from the relationship between elastic modulus and particle size given below (Itasca, 2008).

$$k_n = 4RE_c \tag{3a}$$

$$\bar{k}^n = \frac{\bar{E}_c}{L} \tag{3b}$$

where, k_n = ball stiffness, N/m; R = ball radius, m; E_c = ball elastic modulus, Pa; $\bar{k}^n$ = bond stiffness, Pa/m; $\bar{E}_c$ = bond elastic modulus, Pa; L = centre to centre distance of two balls in contact, m.

In this study, the previously calibrated ball microproperties (K_N = 5×10^4 N/m, k_n/k_s = 1, μ = 1.0) by Sadek et al. (2011) were used. As the elasticity is the intrinsic property of the material, it is more appropriate to use the modulus instead of the stiffness. The ball normal stiffness value from Sadek et al. (2011) was obtained for a uniform particle size of 2 mm. This stiffness was converted to elastic modulus: E_c = 1.25×10^7 Pa according to Equation (3a). Thus, only σ_c and $\bar{E}_c$ were unknown and were to be calibrated.

3.1.3 Virtual tensile test

A virtual fibre with the desired diameter and length was first constructed using balls and bonds as described above. The centre of the first ball of the virtual fibre was set as the origin of the coordinate system and the x-axis was along the centre line of the virtual fibre (Figure 6). To simulate a tensile test, the ball at the origin was fixed by applying a zero velocity boundary condition. All other balls in the virtual fibre are free to

move. A tensile load along the *x*-axis was applied at the free end of the virtual fibre by pulling the last ball at a constant velocity. This model simulates the laboratory tests conducted with the Instron testing system, and it allows altering magnitudes of fibre diameter, length, pulling velocity, and microproperties of the ball and bond.

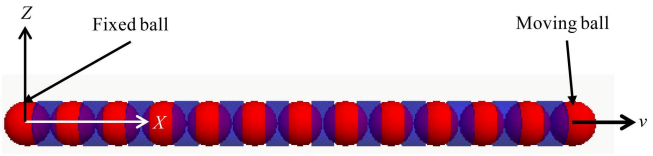

Figure 6 A virtual fibre subjected to a pulling action at a constant velocity

During the virtual testing, the velocity of the last ball will cause increase in the tensile stress within the virtual fibre, more specifically within the cylindrical bonds. The virtual fibre will fail if the maximum tensile stress exceeds the tensile strength of the bond. This concept has been verified in PFC^{3D} using an example of a cantilever beam subjected to a tensile load (Itasca, 2008). Given these facts, the bond strength, σ_c, was envisioned to be equivalent to the maximum stress measured in the tensile tests, while the bond modulus, $\bar{E}_c$, was being calibrated, as described in the model calibration section below.

3.2 Simulation results

3.2.1 Model behaviour

Before calibrations, the behaviour of the model was observed with assumed bond parameters. When a tensile load is applied to a virtual fibre, i.e. when the ball at the free end of the fibre is being pulled at a constant velocity, the virtual fibre is extended. As the virtual fibre continues to be pulled, the stress of the virtual fibre is increasing in a linear fashion and fails suddenly. The extension of the virtual fibre is considered as the displacement of the last ball along the x-axis direction. This displacement and the stress of virtual fibre were monitored and plotted in Figure 7. Although not all load-extension curves from the virtual tests were like those from the laboratory tests shown in Figure 4, the general behaviour of the load increasing with extension and the sudden failure pattern were similar between the virtual and laboratory tests. The virtual fibre is considered to be broken when the detachment between balls within the virtual fibre occurs.

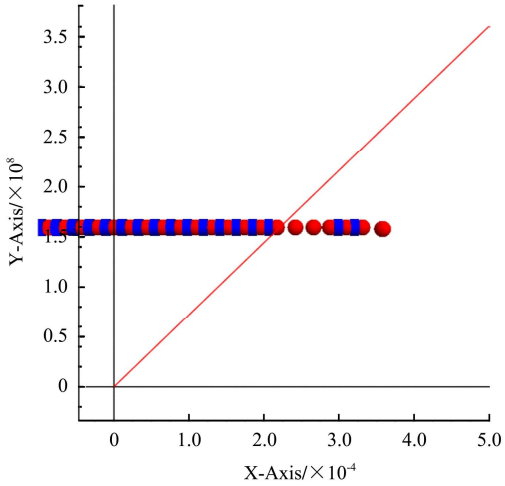

Note: X-Axis is fibre extension, m and Y-Axis is maximum stress, Pa.

Figure 7 A typical load-extension curve from a virtual tensile test

3.2.2 Model calibration

The model input parameters for the retted and unretted fibres are listed in Table 2, and the value of $\bar{E}_c$ was assumed. In running the model for calibrations of $\bar{E}_c$, comparisons in stress were made between simulated and measured fibre stresses at every computing cycle. When the stress of the virtual fibre reaches the maximum stress measured, the extension of the virtual fibre was recorded as the elongation of the virtual fibre, and the simulation was ended. The simulated elongation was recorded for each of the assumed $\bar{E}_c$ values. To assess which assumed value of $\bar{E}_c$ resulted in the elongation which best matched the measured elongation, relative errors between simulations and measurements were calculated using the following equation:

Table 2 Model input parameters for simulations

Model parameters	Unretted	Retted	Source
Length of the fibre, mm	25	25	Same as the fibre samples tested
Diameter of the fibre, mm	0.34	0.30	Average of all the fibre samples
Number of balls in the fibre	74	84	Determined using Equation (2)
Ball elasticity modulus, Pa	1.25×10^7	1.25×10^7	Sadek et al. (2011)
Ball friction	1.0	1.0	Sadek et al. (2011)
Bond normal and shear strength, Pa	3.58×10^8	3.43×10^8	Average maximum stress measured
Diameter of the cylindrical bond, mm	0.34	0.30	Equal to the fibre diameter

$$RE = \frac{|e_m - e_s| \times 100}{e_m} \quad (4)$$

where, RE = relative error, %; e_m = elongation measured, mm; e_s = elongation simulated, mm.

Some of the simulation results are listed in Table 3 to demonstrate how the calibrated $\bar{E}_c$ was selected. As can be seen, fibre elongations were extremely sensitive to $\bar{E}_c$, and increasing $\bar{E}_c$ resulted in increasing of the elongation for both the fibres. Among the assumed values of $\bar{E}_c$, the the best match to the measured elongation was 1.02×10^{10} Pa for unretted hemp and 1.05×10^{10} Pa for retted fibres. The corresponding relative errors were 1.14% and 1.25%. Either increasing or decreasing $\bar{E}_c$ value resulted in a greater relative error.

Table 3 Summary of calibration results using the data from the unretted and retted fibres

Bond modulus, $\bar{E}_c$ /Pa	Unretted			Retted		
	Measured elongation /mm	Simulated elongation /mm	Relative error /%	Measured elongation /mm	Simulated elongation /mm	Relative error /%
9.0×10^9	0.88	0.98	11.36	0.80	0.95	18.75
9.5×10^9	0.88	0.93	5.68	0.80	0.89	11.25
1.02×10^{10}	0.88	0.87	1.14	0.80	0.84	5
1.05×10^{10}	0.88	0.85	3.41	0.80	0.81	1.25
1.10×10^{10}	0.88	0.81	7.95	0.80	0.77	3.75

3.2.3 Effects of fibre length and diameter on fibre elongation

The model can be used to predict elongations for fibres with any lengths and diameters. Here, virtual tensile tests were performed with the calibrated bond modulus. The other model parameters were those for the unretted hemp listed in Table 2. The testing velocity was 2 mm/min, the same as the tensile tests. To examine effects of fibre length on elongation, the virtual tensile tests were performed for five different fibre lengths: 20, 25, 30, 35, and 40 mm with a constant fibre diameter of 0.30 mm. Similarly, virtual tests were performed for five different diameters: 0.20, 0.25, 0.30, 0.35, and 0.40 mm with a constant fibre length of 30 mm to examine effects of fibre diameter on elongation. The simulation results show that elongation is increased linearly (R^2 = 0.99) with the increase of fibre length (Figure 8a). The simulated elongations ranged from 0.69 to 1.39 mm when fibre length varies from 20 to 40 mm. When these elongations were translated to strains, the average strain was 3.48% with a very small standard deviation: 0.02, demonstrating the consistency of the virtual tests over the studied range of fibre length. This result supports the hooks law where the strain rate is constant for a maximum elastic strength of material. Simulation results also showed that the elongation remains fairly constant for all diameters (Figure 8b). This implies that the simulated fibre behaved as anisotropic linear elastic material independent of the fibre diameter. In summary, the results reveal that the calibrated model is reliable for simulating tensile strength of fibre with variable lengths and diameters.

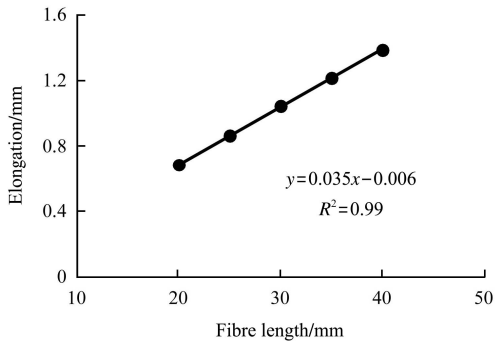

a. Effect of fibre length

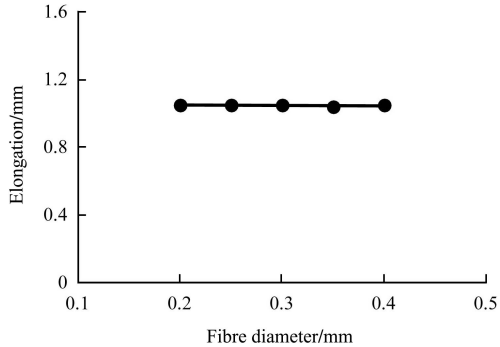

b. Effect of fibre diameter

Figure 8 Simulated elongations for unretted fibre

In the literature, tested fibres used by different researchers were different in length and diameter. As

the elongation of fibre varies with the fibre length, the simulated strain was compared with the literature data. The simulated strain (3.48%) was higher than the average strain for hemp fibre (1.6%) reported by Khan et al. (2011) and that (3.0%) by Duval et al. (2011). However, the simulated strain was within the range (1.3%-5.0%) observed by Munder and Fürll (2004) and Sankari (2000).

4 Conclusions

Hemp fibres can be simulated with the numerical model developed using PFC^{3D}, commercial discrete element software. A virtual fibre, formed using spherical particles connected with bonds implemented in the PFC^{3D} parallel bond model, reflects tensile behaviours of a real fibre. Specifying a given velocity to one end of the virtual fibre represents tensile load adequately, while the other end of the virtual fibre is affixed. Among the several microproperties for particles and bonds of a virtual fibre, the bond microproperties in the normal direction are more critical as they determine the tensile strength of the virtual fibre. The calibrated bond modulus using the laboratory tensile test data was 1.02×10^{10} Pa for unretted fibre and 1.05×10^{10} Pa for retted fibre. The simulated result showed that under a tensile load, elongation of a fibre increases linearly with the increase of the fibre length, while the elongation remains nearly constant for different fibre diameters. The model is capable of simulating numerous tensile behaviours of fibre, including load-extension curve, maximum stress, and elongation. The model allows users to alter diameter and length of the fibre.

Acknowledgements

This work was supported by the Natural Sciences and Engineering Research Council of Canada (NSERC). The authors thank Dr. Stefan Cenkowski for providing the fibre testing system.

References

Duval, A., A. Bourmauda, L. Augier, and C. Baley. 2011. Influence of the sampling area of the stem on the mechanical properties of hemp fibers. Materials Letters, 65: 797-800.

Asaf, Z., D. Rubinstein, and I. Shmulevich. 2007. Determination of discrete element model parameters required for soil tillage. *Soil & Tillage Research,* 92(1-2): 227-242.

Beckermann, G. W., and K. L. Pickering. 2008. Engineering and evaluation of hemp fiber reinforced polypropylene composites: Fiber treatment and matrix modification. *Composites: Part A,* 39: 979-988.

Bledzki, A. K., S. Reihmane, and J. Gassan. 1996. Properties and modification methods for vegetable fibers for natural fiber composites. *Journal of Applied Polymer Science* 59(8): 1329-1336.

Bocsa, I., and M. Karus. 1997. The cultivation of hemp, Sebastopol, California: Chelsea Green Publishing Company.

CGSB. 2001. Conditioning textile materials for testing. Canadian General Standards Board and Standards Council of Canada, CAN/CGSB-4.2 no. 2-M88.

Chang, C. S., C. L. Liao, and Q. Shi. 2003. Elastic granular materials modeled as first order strain gradient continua. *International Journal of Solids and Structures,* 40(21): 5565-5582.

Coetzee, C. J., and D. N. J. Els. 2009. Calibration of discrete element parameters and the modelling of silo discharge and bucket filling. *Computers and Electronics in Agriculture* 65(2): 198-212.

Cundall, P. A., and O. D. L. Strack. 1979. A discrete numerical model for granular assemblies. *Geotechnique,* 29(1): 47-65.

Cundall, P. A., and O. D. L. Strack. 1982. Modeling of microscopic mechanics in granular material. In: J. T. Jenkins, and M. Satake (Eds.), *Mechanics of Granular Materials: New Models and Constitutive Relations* (pp. 113–149). Amsterdam: Elsevier.

Djordjevic, N. 2003. Discrete element modeling of the influence of lifters on powder draw of tumbling mills. *Minerals Engineering,* 16(4): 331-336.

Garcia, C., D. D. Jaldon, and M. R. Vignon. 1998. Fibers from semi-retted hemp bundles by steam explosion treatment. *Biomass and Bioenergy,* 14(3): 251-260.

Hobson, R. N., D. G. Hepworth, and D. M. Bruce. 2001. Quality of fiber separated from unretted hemp stems by decortication. *Journal of Agricultural Engineering Research,* 78(2): 153-158.

Itasca. 2008. PFC^{3D} (Particle Flow Code in 3 Dimensions), verification problems and example applications, version 4.0. Minneapolis, MN, USA: Itasca Consulting Group, Inc.

Keller, A., M. Leupin, V. Mediavilla, and E. Wintermantel. 2001.

Influence of the growth stage of industrial hemp on chemical and physical properties of the fibres. *Industrial Crops and Products,* 13(1): 35-48.

Khan, M. R., Y. Chen, T. Belsham, C. Lague, H. Landry, Q. Peng, and W. Zhong. 2011. Fineness and tensile properties of hemp (Cannabis sativa L.) fibers. *Biosystems Engineering,* 108(1): 9-17.

Kymäläinen, H. R. 2004. Quality of *Linum usitissimum* L. (flex and linseed) and *Cannabis sativa* L. (hemp fiber) during the production chain of fiber raw material for thermal insulation. Helsinki, Finland: Department of Agricultural Engineering and Household Technology, University of Helsinki.

Landry, H., C. Laguë, and M. Roberge. 2006. Discrete element representation of manure products. *Computers and Electronics in Agriculture,* 51 (1-2): 17-34.

Lilholt, H., and J. M. Lawther. 2000. Natural organic fibers. In A. Kelly, and C. Zweben (Eds.), *Fiber reinforcements and general theory of comprehensive composite materials* (pp. 303-325). Amsterdam: Elsevier.

Mak, J., Y. Chen, and M. A. Sadek. 2012. Determining parameters of a discrete element model for soil–tool interaction. *Soil & Tillage Research,* 118(2012): 117-122.

McDowell, G. R., and O. Harireche. 2002. Discrete element modeling of yielding and normal compression of sand. *Geotechnique,* 52(4): 299-304.

Mediavilla, V., M. Leupin, and A. Keller. 2001. Influence of the growth stage of industrial hemp on the yield formation in relation to certain fiber quality traits. *Industrial Crops and Products,* 13 (2001): 49-56.

Munder, F., and C. Fürll. 2004. Effective processing of bast fiber plants and mechanical properties of the fibers. ASAE/CSAE Annual International Meeting, Ottawa, Ontario, Canada.

Munder, F., and C. Fürll. 2004. Effective processing of bast fiber plants and mechanical properties of the fibers. *ASAE/CSAE Annual International Meeting*, Ottawa, Ontario, Canada.

Pierce, M. E. 2004. PFC^{3D} modeling of inter-particle percolation in caved rock under draw. In Y. Shimizu, R. Hart, and P. A. Cundall (Eds.), *Numerical Modeling in Micromechanics via Particle Methods* (pp. 149-156). Kyoto: Taylor and Francis.

Potyondy, D. O., and P. A. Cundall. 2004. A bonded-particle model for rock. *International Journal of Rock Mechanics and Mining Science,* 41(8): 1329-1364.

Rowell, R. M., J. S. Han and J. S. Rowell. 2000. Characterization and Factors Effecting Fiber Properties. *Natural Polymers and Agrofibers Composites* 115-134. ISBN: 85-86463-06-X.

Sadek, M. A., Y. Chen, C. Laguë, H. Landry, Q. Peng, and W. Zhong. 2011. Characterization of the shear properties of hemp using discrete element method. *Transactions of the ASABE,* 54(6): 2279-2285.

Sakaguchi, F., M. Suzuki, J. F. Favierand, and S. Kawakami. 2001. Numerical simulation of the shaking separation of paddy and brown rice using the discrete element method. *Journal of Agricultural Engineering Research,* 79(3): 307-315.

Sankari, H. 2000. Comparison of bast fiber yield and mechanical fiber properties of hemp (*Cannabis sativa* L.) cultivars. *Industrial Crops and Products,* 11(1): 73-84.

Saville, B. P. 1999. Physical Testing of Textiles. Textile Institute. Manchester, England. Woodhead publishing.

Tanaka, H., M. Momozo, A. Oida, and M. Yamazaki. 2000. Simulation of soil deformation and resistance at bar penetration by distinct element method. *Journal of Terramechanics,* 37 (1): 41-56.

Vu-Quoc, L., X. Zhang, and O. R. Walton. 2000. A 3-D discrete-element method for dry granular flows of ellipsoidal particles. *Computer Methods in Applied Mechanics and Engineering,* 187 (3-4): 483-528.

Williams, G. I., and R. P. Wool. 2000. Composites from natural fibers and soy oil resins. *Applied Composite Materials,* 7(5): 421-432.